The corkscrew instability of a Fréedericksz domain wall in a nematic liquid crystal

New Journal of Physics
An Institute of Physics and Deutsche Physikalische Gesellschaft Journal

The corkscrew instability of a Fréedericksz domain wall in a nematic liquid crystal

Alberto de Lózar Muñoz, Thomas Bock, Matthias Müller, Wolfgang Schöpf and Ingo Rehberg

Experimentalphysik V, Universität Bayreuth, D-95440 Bayreuth, Germany
E-mail: wolfgang.schoepf@uni-bayreuth.de

New Journal of Physics **5** (2003) 63.1–63.12 (http://www.njp.org/)
Received 10 January 2003, in final form 26 March 2003
Published 6 June 2003

Abstract. A liquid crystal with slightly positive dielectric anisotropy is investigated in the planar configuration. This system allows for competition between electroconvection and the homogeneous Fréedericksz transition, leading to a rather complicated bifurcation scenario. We report measurements of a novel instability leading to the 'corkscrew' pattern. This state is closely connected to the Fréedericksz state as it manifests itself as a regular modulation along a Fréedericksz domain wall, although its frequency dependence indicates that electroconvection must play a crucial role. It can be understood in terms of a pitchfork bifurcation from a straight domain wall. Quantitative characterization is performed in terms of amplitude, wavelength and relaxation time. Its wavelength is of the order of the probe thickness, while its ondulation amplitude is an order of magnitude smaller. The relaxation time is comparable to the one obtained for electroconvection.

Contents

PII: S1367-2630(03)58130-7

1. Introduction

For the study of pattern formation under non-equilibrium conditions, convection in fluids is a classical example due to its similarity to numerous pattern-forming phenomena in nature [1]. The most prominent system is Rayleigh–Bénard convection in simple fluids, where a horizontal fluid layer is heated from below. If the temperature difference across the layer exceeds a certain threshold value, the system undergoes a bifurcation from a uniform and motionless state to a convective state. Convection may occur in the form of regular patterns, e.g. stripes, squares or spirals, but also in the form of chaotic motion [2].

Another system that has been investigated intensively both theoretically and experimentally in the context of symmetry-breaking instabilities is a nematic liquid crystal under the influence of an alternating electric field [3]–[5]. Depending on the frequency and amplitude of the applied field in connection with the size and sign of certain material parameters, a huge variety of convective states may arise [5, 6]. It turns out that the primary instabilities show a high degree of universality for which a full classification has been achieved [1]. A full classification of the secondary instabilities destabilizing the primary patterns, however, seems a tremendous task, except for the quasi-one-dimensional case [7] where they have been analysed in detail for Rayleigh–Bénard convection in simple fluids [8]. Thus a systematic study of the nonlinear behaviour of nematic liquid crystals is highly desirable.

A nematic liquid crystal is an intrinsically anisotropic fluid with uniaxial symmetry which can be described macroscopically by anisotropic material parameters. The molecules have a tendency to align parallel to each other, leading to a preferred axis characterized by the director field $\boldsymbol{n}$, and thus to a long-range order in the equilibrium state. Important for the interaction with an electric field and with free charges are the dielectric anisotropy, ϵ_a, and the anisotropy of the electrical conductivity, σ_a, respectively. For $\epsilon_a > 0$ ($\epsilon_a < 0$) the director has a tendency to align parallel (perpendicular) to the applied field. For $\sigma_a > 0$ ($\sigma_a < 0$) charges move preferably parallel (perpendicular) to the director. In the planar configuration, the liquid crystal forms a thin fluid layer confined between two transparent electrodes, with the director being aligned in a preferred direction in the layer plane by a suitable treatment of the electrodes. An ac-voltage $U(t) = \sqrt{2}U_{rms}\cos(2\pi f t)$ is applied across the electrodes, where the rms-amplitude U_{rms} and the frequency f serve as the main control parameters of the system.

When increasing the voltage U_{rms} beyond a certain critical value $U_c(f)$, the homogeneous and motionless basic state, with the director oriented parallel to the boundaries, becomes unstable. For materials with $\epsilon_a < 0$ and $\sigma_a > 0$, the phenomenon of electroconvection is encountered at threshold [9]. The most prominent primary pattern consists of normal rolls, where the roll axis is perpendicular to the director field. In addition, oblique rolls can be observed in liquid crystals with sufficiently low ϵ_a for small driving frequencies [6, 10]. For a material with $\epsilon_a > 0$, on the other hand, the homogeneous Fréedericksz transition occurs for a critical voltage $U_f = \pi\sqrt{k_{11}/\epsilon_0\epsilon_a}$ which is independent of the driving frequency [3]. Here, k_{11} is the splay elastic constant of the liquid crystal.

When increasing the driving voltage in the case of electroconvection, the primary patterns destabilize via secondary instabilities, such as, for example, the long-wave zigzag or skewed-varicose patterns [11, 12]. For certain frequencies, a homogeneous instability can also be observed, which is caused by a twist in the director field leading to abnormal rolls [13, 14]. These secondary instabilities typically give rise to the formation of domains in the liquid crystal, so that the two possible and equivalent states are separated by domain walls.

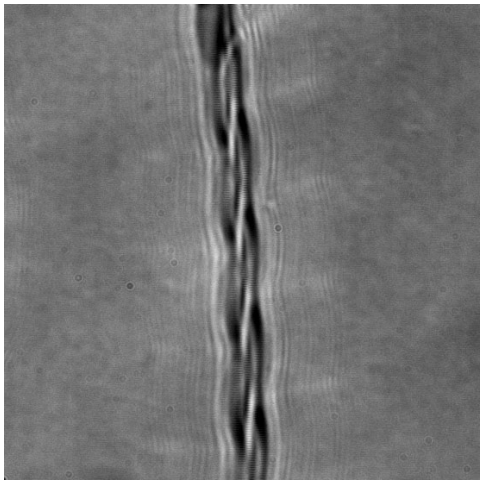

Figure 1. Magnification of the corkscrew pattern. The shadowgraph technique gives the impression of a chiral object.

This paper is concerned with the case that the Fréedericksz transition and a convective instability can be observed in the same system, which is possible for nematics with weakly positive ϵ_a and positive σ_a. The competition between the two instability mechanisms promises an interesting bifurcation scenario. For certain frequencies, for example, we find a convective roll pattern as the primary threshold, which upon increasing the voltage develops into a Fréedericksz state characterized by the presence of domain walls. Although the birefringence method indicates a 'normal' Fréedericksz state, it is modulated by convection, which must be present near the domain walls. We speculate that this is the reason for the stability of so many domain walls, which otherwise would be expected to decay until only one wall is left. Typical for this state is the appearance of a zigzag instability along the domain walls, similar to the one observed in a liquid crystal experiment using homeotropic alignment and a combination of electric and magnetic fields [15]. A further increase of the voltage destabilizes the domain walls into a novel state that, due to its peculiar appearance, we have termed the 'corkscrew' pattern. Figure 1 shows a strong magnification of such a state. The caustic line produced by the shadowgraph method gives the impression of a chiral object, although this does not necessarily mean that the underlying director field is chiral as well. Indeed, we do not have a model for the director field yet.

An example sequence for increasing voltage is shown from left to right in figure 2. The preferred director orientation is in the horizontal direction, i.e. roughly perpendicular to the lines. The zigzag instability of the domain walls can be seen in the middle part of figure 2, while it is obvious from the right part, that the corkscrew pattern is a new state different from the zigzag lines. It rather appears as a further instability on top of the zigzag pattern, but may also occur along straight domain walls, as will be discussed later. Depending on the driving voltage and frequency, the corkscrew state (right part of figure 2) may be rather dynamic, as can be seen from the accompanying MPEG movie.

Our goal is to characterize the corkscrew pattern in terms of its range of existence in phase space and to measure its critical voltage and wavelength as functions of frequency, so as to foster its theoretical description. It turns out that the occurrence of the pattern depends strongly on the

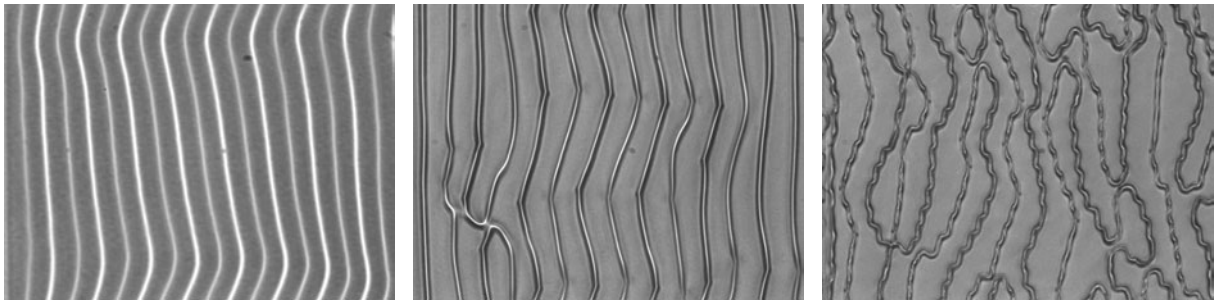

Figure 2. A convective roll state at $f = 20$ Hz near the primary threshold (left, $U_{rms} = 12.79$ V). For increasing voltage, it develops into a Fréedericksz state (middle, $U_{rms} = 19.70$ V) and eventually into the corkscrew pattern (right, $U_{rms} = 37.77$ V). An animation of the final state is provided.

angle between the domain walls and the preferred director alignment, and also on the number of domain walls present. Therefore, we will initially investigate this pattern for a single, isolated domain wall that is perpendicular to the director field.

2. Experimental set-up

For the experiments presented in this paper we use a commercial nonpolar azoxy mixture of liquid crystals, distributed by Merck under the name 'ZLI-3086'. According to the data sheet[1], this material has a dielectric anisotropy of $\epsilon_a \approx 0.1$ which enables us to investigate both electroconvection and the Fréedericksz transition in the same system. Using dynamic-scanning calorimetry apparatus, we found that the nematic phase of our 'ZLI-3086' probe occurs in the temperature range $T = -20$–$76\,^{\circ}$C. Our measurements have been performed at a temperature of $22\,^{\circ}$C with a long-term stability of ± 5 mK. In order to achieve sufficient electrical conductivity we have to dope this liquid crystal with iodine, as the pure material is essentially electrically insulating with no free charges to trigger the Carr–Helfrich mechanism [16] leading to electroconvection.

We use the standard experimental set-up as described e.g. in [6, 14]. The liquid crystal is embedded between two parallel transparent electrodes (glass plates with an ITO layer [17]). The surfaces of the electrodes are coated with a polymer and rubbed in one direction to produce the planar alignment. The rub direction defines the x-axis, with the y-axis being perpendicular to x in the layer plane. The thickness of the probe $d = 30 \pm 4$ μm is determined by the spacer material which separates the two glass plates in the z-direction. A detailed description of the sample preparation is presented elsewhere [18]. One of the electrodes has been prepared by an etching process so that only narrow channels of ITO remain along the y-direction. For our experiments, we use a channel with a width of 0.6 mm. The etching procedure introduces a slight inhomogeneity of the electric field which, due to our large width-to-height ratio of 20, is confined to the vicinity of the channel boundaries. The measurements discussed in this paper always take place in the homogeneous (inner) region of the channel. As a further result of the etching process, convection takes place primarily inside these channels, with a smooth but narrow transition to a convectionless state outside the channels [19].

[1] Merck data sheet for 'ZLI-3086', Rev. Date: 29.01.1999, Merck KGaA, Darmstadt, Germany.

A sinusoidal ac-voltage $U(t) = \sqrt{2}U_{rms}\cos(2\pi f t)$ is applied across the electrodes by means of a waveform generator. We observe the appearing patterns under a polarizing microscope and record them with a CCD camera connected to a frame grabber card. The images have a physical size of $552 \times 417\ \mu\text{m}^2$ and are digitized with a spatial resolution of 640×484 pixels into 256 grey scales at a rate of 60 images per second. Both electroconvection and the Fréedericksz domain walls are visualized using the shadowgraph method [20, 21]. The main feature here is the transformation of a spatially modulated refractive index, caused by the deflection of the director angle, into quantitative light intensity information resulting from geometrical optics. The Fréedericksz transition itself is observed using the birefringence technique, where the probe is between two crossed polarizers both of which define an angle of 45° with respect to the preferred director orientation (here the x-axis) [22, 23]. In order to obtain a reproducible shadowgraph intensity, it is necessary to use a stroboscopic illumination, because the director field varies slightly in time with the external frequency. For that purpose, our sample is illuminated by an LED that flashes with the frequency of the driving ac-voltage [24]. The phase and duration of the flashes are computer controlled, so that our shadowgraph images always result from the same phase of the director with respect to the driving force.

3. Phase diagram of 'ZLI-3086'

The Fréedericksz threshold $U_f = \pi\sqrt{k_{11}/\epsilon_0\epsilon_a}$ is independent of the driving frequency f, while the convective threshold $U_c(f)$ increases monotonically with increasing frequency. When $\epsilon_a > 0$ is sufficiently small, as for 'ZLI-3086', it is possible to find $U_c(f) < U_f$ for $f < f_{C2}$, where f_{C2} is a codimension-2 point separating the two bifurcation branches.

The onset of the primary instabilities has been measured by starting from a subcritial state and then increasing the voltage in small steps for fixed frequency. After each voltage step, the system is given sufficient time to relax into its new state before a measurement is taken. Electroconvection manifests itself in form of parallel stripes along the y-direction being periodic in x, which develop from the unstructured ground state above threshold (see e.g. [6]). When observing the system between crossed polarizers, the Fréedericksz transition is indicated by a homogeneous change in the light intensity (see e.g. [25]). The results of our measurements are presented as functions of the frequency in figure 3, with the wavenumber being shown in the upper diagram and the threshold voltage in the lower diagram. The open circles correspond to the onset of electroconvection. The open square indicates the homogeneous Fréedericksz transition with measurements made up to 300 Hz in steps of 30 Hz. As expected we observe no frequency dependence within this range. Obviously, the wavenumber is zero in this case. We measure $U_f = 13.50$ V for the Fréedericksz threshold and find the codimension-2 point at $f_{C2} = 30$ Hz.

The curves in figure 3 are fits of a single-mode model to our data [10, 26]. This model contains, in principle, nine adjustable parameters, however, the anisotropy of the electrical conductivity, the dielectric permittivities and the Fréedericksz threshold have been measured independently, so that we are left with five parameters[2]. With this model, the threshold voltage

[2] The fixed parameters are $\sigma_a = 0.4 \times 10^{-8}\ \Omega^{-1}\ \text{m}^{-1}$, $\epsilon_\perp = 2.8$, $\epsilon_a = 0.06$ and $U_f = 13.50$ V. The fitted parameters are $\sigma_\perp = 0.28 \times 10^{-8}\ \Omega^{-1}\ \text{m}^{-1}$, $k_{33}/k_{11} = 1.84$, $\alpha_3/\alpha_2 = 15.1 \times 10^{-3}$, $\eta_2/\alpha_2 = -2.99 \times 10^{-2}$ and $(\alpha_1 + \eta_1 + \eta_2)/\alpha_2 = -1.27$. For further details, see e.g. [10].

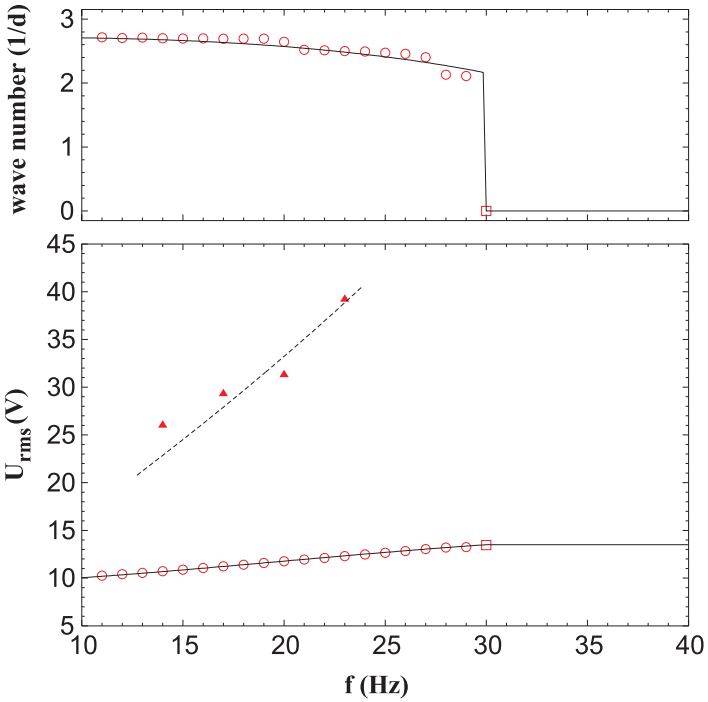

Figure 3. Phase diagram for our liquid crystal 'ZLI-3086'. The open circles and squares indicate the onset of electroconvection and the Fréedericksz transition, respectively. The upper diagram shows the wavenumbers of these primary instabilities. The triangles are our actual measurement points for the onset of the corkscrew instability, as explained in detail in section 4. The solid curves are fits of a theoretical model, while the dotted line is only a guide to the eye.

and the wavenumber curves are fitted at the same time, both of which are well represented by the fit.

For the primary Fréedericksz transition ($f > f_{C2}$), the important feature in our channel geometry is that due to symmetry-breaking effects introduced by the channel boundaries, we always find a Fréedericksz domain wall roughly in the middle of the channel[3]. This wall separates the two symmetric Fréedericksz states. When we increase the voltage, this domain wall essentially remains as it is, except for very high voltages ($U_{rms} > 60$ V) when it breaks up into two disclination lines, a behaviour that is well understood [3].

Although various secondary instabilities have been observed in this system, the full phase diagram has not been investigated in a systematic way yet. Our goal is to characterize the corkscrew pattern experimentally for a single isolated domain wall that is perpendicular to the director, i.e. parallel to the y-direction. The full triangles in figure 3 are the results of such measurements of the corkscrew threshold as discussed in the following section.

[3] When applying an electric field, the channel geometry introduces a pretilt near the channel boundaries, which is stronger than any pretilt that may result from the glass plate rubbing procedure. Thus we are able to prepare reproducible Freedericksz domain walls.

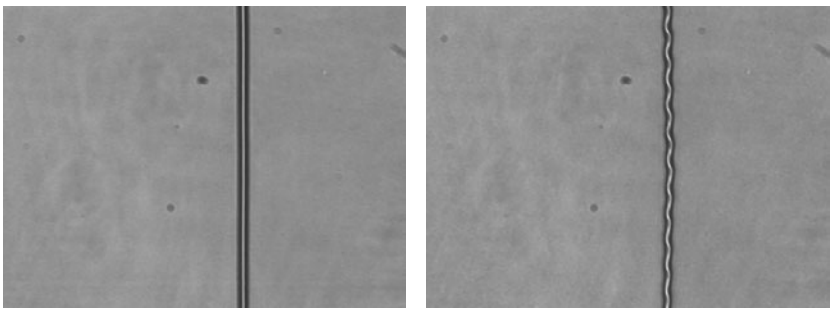

Figure 4. A single domain wall prepared at $f = 300$ Hz and $U_{rms} = 34.82$ V (left) develops into a corkscrew pattern (right) after changing the frequency to $f = 20$ Hz. An animation of the transition is also provided. The height and width of the images are 0.31 and 0.41 mm, respectively. The right channel boundary is 0.22 mm away from the wall, while the left boundary is 0.38 mm away. Both are outside of the field of view.

4. Corkscrew instability

4.1. Jump procedure

The instability of a single Fréedericksz domain wall against the corkscrew modulation is investigated as follows. We first prepare a Fréedericksz state with a single domain wall in one of the narrow channels (the left part of figure 4) at a frequency of 300 Hz, which is well above the codimension-2 frequency $f_{C2} = 30$ Hz. The applied voltage is, e.g. 35 V, which would lead to a corkscrew pattern for a sufficiently low frequency[4]. Now we suddenly decrease the frequency to $f = 20$ Hz, with the voltage kept constant. In this way, the system is brought into the corkscrew range. The final pattern (the right part of figure 4; an MPEG movie of the evolution spanning over 5 s is also provided) typically develops within a few seconds. With this procedure, we are able to investigate the corkscrew pattern on an isolated line, where it is not influenced by neighbouring patterns. Such a state is stable for about 20 s before further lines enter from the far ends of the channel. As soon as they come within a certain distance of each other, they tend to interact in an irregular way, leading to a rather dynamic scenario. In order to avoid this complication, the system is brought back into the stable Fréedericksz regime in less than 20 s, i.e. we increase the frequency back to 300 Hz with the voltage still constant at 35 V. In this way, we can typically recover our initial single domain wall as a starting point for the next experiment.

4.2. Extraction of the domain wall

During jump procedures as just described, we follow the temporal evolution of the various states with our CCD camera. Typically, the camera is started upon initialization of a jump (either in frequency or in voltage) and then samples images at a rate of 60 full frames s^{-1}. Our first goal therefore is to extract the domain walls and corkscrew modulations as shown in figure 4 from

[4] In an extended bulk geometry domain walls are also present, however, it would always be possible to find a sufficiently large location within the probe which is free of such walls. On the other hand, it would be impossible to consistently prepare a domain wall in the same spot, as it is used for our investigations here.

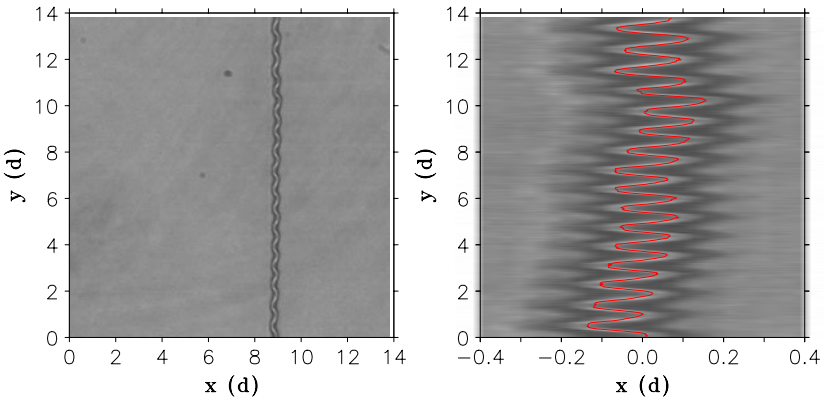

Figure 5. Shadowgraph image of a corkscrew line shown on different x-scales. The red line overlaid in the right image has been obtained by the procedure described in the text.

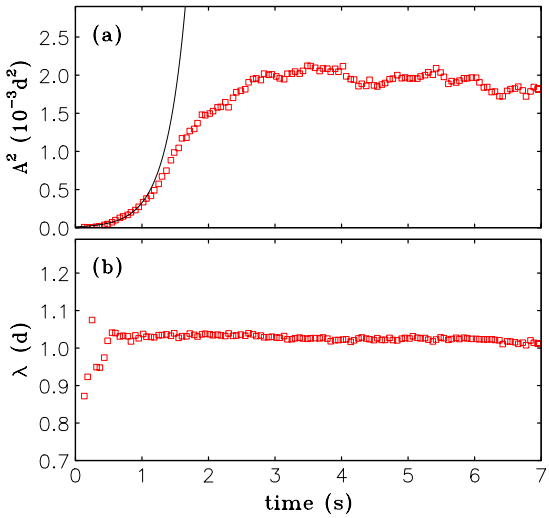

Figure 6. Evolution of the Fourier intensity A^2 (a) and wavelength λ (b) of the corkscrew pattern as functions of time at 31.20 V for a jump from 300 to 17 Hz. The curve is a fit to an exponential growth. The resulting equilibrium amplitude $A_{cs} = 0.043$ d and wavelength $\lambda = 1.02$ d are obtained by averaging the data points between 5 and 7 s.

such images so that they can be further analysed in terms of amplitude and wavelength. This means, we need to transform the light intensity information $I(x, y)$ from the CCD camera into a line $x_l = x_l(y)$, where x_l is the modulation of the pattern as a function of the coordinate y along the line.

When we analyse the horizontal lines $I(x)$ of images such as presented in figure 4, it turns out that the actual pixel representing the centre of the domain wall is not necessarily an absolute intensity maximum along such a line, but rather a local one. Therefore, we first transform the line $I(x)$ into

$$I_m(x) = \frac{I(x)}{(\sum_{i=1}^{4} \max(I(x+i), I(x-i)))^2} \tag{1}$$

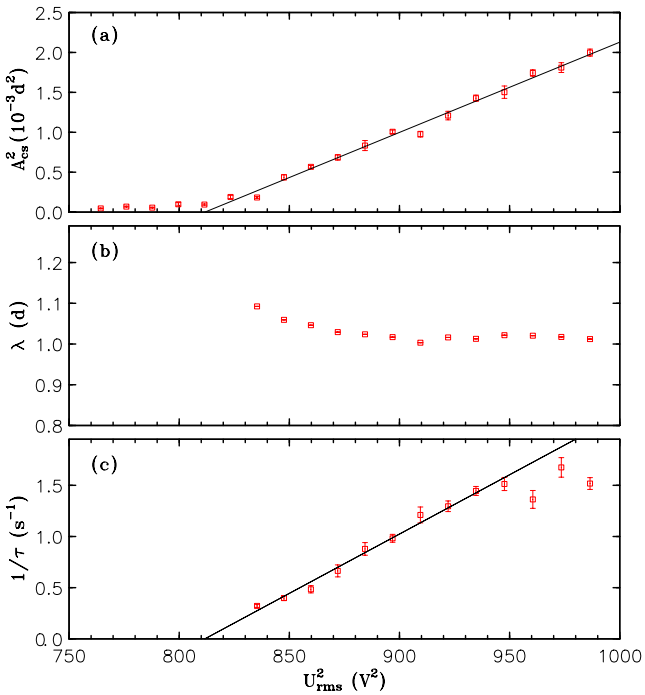

Figure 7. Fourier intensity A_{cs}^2 (a), wavelength λ (b) and growth rate $1/\tau$ (c) of the corkscrew pattern as functions of U_{rms}^2 for $f = 17$ Hz. The squares have been extracted from our measurements, while the lines result from the fit of a theoretical model as discussed in section 5.

which emphasizes the contrast of a pixel with respect to its vicinity. In a second step, this function is smoothed by a finite impulse response low-pass filter [27] with symmetric coefficients $\frac{1}{9}$, $\frac{2}{9}$, $\frac{3}{9}$, $\frac{2}{9}$, $\frac{1}{9}$ around the centre point, resulting in $\bar{I}(x)$. The line $x_l(y)$ can then be extracted as the maxima of parabolic interpolations of $\bar{I}(x)$ for all y in the region of interest. The procedure is illustrated in figure 5. The left part shows the original shadowgraph image of the corkscrew pattern. The right part shows the image again on an extended x-scale, with the extracted line overlaid in red.

To finally obtain the amplitude A and wavelength λ, the line is prepared such that it has roughly the same phase at both ends, discarding the remainder. The slope is then subtracted before we perform a discrete Fourier transform of the line. As this does not produce a single peak, we estimate the amplitude of the pattern by adding the Fourier intensities for a range of wavenumbers around the peak. The wavenumber itself is calculated as the weighted average over this wavenumber range.

4.3. Measurements for increasing amplitudes

In order to measure the stability characteristics of a single domain wall at a certain frequency f, we apply the procedure described in section 4.1 repeatedly for different voltages. In the concrete case of 17 Hz (the second triangle from the left in figure 3), we prepare a domain wall at 300 Hz. Upon suddenly decreasing the frequency to 17 Hz at constant voltage, we start the data acquisition procedure as described in section 4.2 and follow the time evolution of the line

for 7 s, after which the pattern is sufficiently stationary. We then jump back to the initial values at 300 Hz.

For every jump, a time series of images of the domain wall is obtained. The line representing the domain wall and its modulation are extracted from each image as described in section 4.2, so that we get the Fourier intensity A^2 and wavelength λ of the modulation of the line (in units of d^2 and d, respectively) as functions of time. This is shown in figure 6 for a jump from 300 to 17 Hz at 31.20 V. Assuming an exponential increase after the jump, we fit a function of the form $A^2 = A_0^2 \exp(2t/\tau)$ to the data. The fit is shown by the curve in figure 6 and yields the growth rate $1/\tau$. After about 4 s, the amplitude and wavelength of the pattern have relaxed onto their equilibrium values which we obtain by averaging the data between 5 and 7 s. This procedure is repeated for all voltages that were used to jump from 300 to 17 Hz. The resulting squared amplitude, wavelength and growth rate of the corkscrew pattern are shown as functions of U_{rms}^2 in figure 7. The lines are fits of a theoretical model and will be discussed in the following section.

5. Discussion and summary

Although the squared equilibrium amplitude A_{cs}^2 of the corkscrew pattern as shown by the open squares in figure 7(a) increases with increasing voltage, there does not seem to be a perfectly sharp transition point which may be due to an imperfect bifurcation or to our experimental uncertainties. The best indication for the critical voltage is given by the growth rate $1/\tau$ shown in figure 7(c). As expected it decreases when approaching the critical value from above and approaches zero at the point of instability.

In order to extract the critical value from such data, we conclude that the corkscrew pattern results from an instability breaking the translational symmetry along the quasi-one-dimensional domain wall. Thus it falls into the I_s class of pattern forming instabilities as introduced by Cross and Hohenberg [1], so that the amplitude A of the corkscrew modulations should obey the following bifurcation model:

$$\tau_0 \partial_t A = \varepsilon A - A^3/A_0^2, \tag{2}$$

where the sign of the nonlinear term is motivated by the experimental observations. Following normal convention, we use $\varepsilon = (U_{rms}^2 - U_c^2)/U_c^2$ as the control parameter for the instability. τ_0 is a typical timescale and A_0 accounts for the nonlinear saturation. For the linear growth rate, equation (2) leads to $A = A_0 \exp(t/\tau)$ with $\tau = \tau_0/\varepsilon$, so that $1/\tau$ as shown in figure 7(c) should increase linearly with increasing U_{rms}^2. Such a linear fit is represented by the solid line, yielding a relaxation time of $\tau_0 \approx 0.11$ s at 17 Hz, with a slight variation for other frequencies. This value is very similar to the one expected for electroconvection ($\tau_0 \approx 0.13$ for MBBA [26]), which leads us to believe that the occurrence of the corkscrew pattern is closely connected to electroconvection. The fit also gives the critical value for the onset of the corkscrew pattern as $U_c = 28.49$ V at this particular frequency of 17 Hz. U_c as a function of the frequency is represented by the four triangles in figure 3.

For the equilibrium amplitude, equation (2) leads to $A_{cs}^2 = \varepsilon A_0^2$. With U_c fixed at the value obtained from the growth rate, a fit of this expression to the experimental data is given by the

line in figure 7(a)[5]. This fit yields the scale $A_0 \approx 0.1$ d of the corkscrew ondulations.

The wavelength λ shown in figure 7(b) increases slightly for decreasing voltage, and is not defined below the bifurcation point. It is interesting to note, that λ is of the order of the cell thickness d, which indicates that the corkscrew pattern is a three-dimensional instability, and not just a modulation in the x–y-plane. As seen above, the amplitude scale A_0 of the corkscrew pattern is typically an order of magnitude smaller than the wavelength.

In summary, we have presented measurements of a novel instability that occurs in nematic liquid crystals with slightly positive dielectric anisotropy. The instability seems to be the result of a competition between electroconvection and the homogeneous Fréedericksz transition. We have shown that it can be described in terms of a pitchfork bifurcation from a straight Fréedericksz domain wall. As a further step, we intend to find the full range of existence of the corkscrew pattern inside the voltage–frequency phase space. We hope that our quantitative investigations will foster a theoretical modelling of this pattern.

References

[1] For a comprehensive review, see
Cross M C and Hohenberg P C 1993 *Rev. Mod. Phys.* **65** 851
[2] For a review, see
Bodenschatz E, Pesch W and Ahlers G 2000 *Annu. Rev. Fluid Mech.* **32** 709
[3] de Gennes P G 1974 *The Physics of Liquid Crystals* (Oxford: Clarendon)
Chandrasekhar S 1977 *Liquid Crystals* (Cambridge: Cambridge University Press)
[4] For a review, see
Buka A and Kramer L (ed) 1996 *Pattern Formation in Liquid Crystals* (Berlin: Springer)
[5] For further reviews, see
Kramer L and Pesch W 1995 *Annu. Rev. Fluid Mech.* **27** 515
Kai S and Zimmermann W 1989 *Prog. Theor. Phys. Suppl.* **99** 458
[6] Rehberg I, Winkler B L, de la Torre Juárez M, Rasenat S and Schöpf W 1989 *Adv. Solid State Phys.* **29** 35
[7] Coullet P and Iooss G 1990 *Phys. Rev. Lett.* **64** 866
[8] Busse F H 1978 *Rep. Prog. Phys.* **41** 1929
[9] Dubois-Violette E, de Gennes P G and Parodi O 1971 *J. Physique* **32** 305
[10] Kramer L and Pesch W 1996 *Pattern Formation in Liquid Crystals* ed A Buka and L Kramer (Berlin: Springer)
[11] Ribotta R, Joets A and Lei L 1986 *Phys. Rev. Lett.* **56** 1595
[12] Braun E, Rasenat S and Steinberg V 1991 *Europhys. Lett.* **15** 579
Nasuno S and Kai S 1991 *Europhys. Lett.* **14** 779
[13] Plaut E, Decker W, Pesch W, Rossberg A, Kramer L, Belaidi A and Ribotta R 1997 *Phys. Rev. Lett.* **79** 2367
[14] Rudroff S, Zhao H, Kramer L and Rehberg I 1998 *Phys. Rev. Lett.* **81** 4144
Rudroff S, Frette V and Rehberg I 1999 *Phys. Rev.* E **59** 1814
[15] Chevallard C, Clerc M, Coullet P and Gilli J-M 2000 *Eur. Phys. J.* E **1** 179
Chevallard C, Nobili M and Gilli J-M 2001 *Liq. Cryst.* **28** 179
[16] Carr E F 1969 *Mol. Cryst. Liq. Cryst.* **7** 253
Helfrich W 1969 *J. Chem. Phys.* **51** 4092

[5] If we use U_c instead as a free fit parameter, we obtain a critical value of $U_c = 28.51$ V which in this case is in almost perfect agreement with the value we get from the growth rate. To be consistent in our measurements and to avoid any ambiguity, we have always used the growth rate for extracting the critical value, since in general it yields the threshold with a higher precision.

[17] Merck Display Technologies, F030 Rev. 6 (970924) *Coatings for Flat Panel Displays* (Merck Display Technologies Ltd, Taiwan)
[18] Bock T M, Blaesing J, Frette V and Rehberg I 2000 *Rev. Sci. Instrum.* **71** 2800
[19] Peacock T, Binks D J and Mullin T 1999 *Phys. Rev. Lett.* **82** 1446
[20] Rasenat S, Hartung G, Winkler B L and Rehberg I 1989 *Exp. Fluids* **7** 412
Rehberg I, Hörner F and Hartung G 1991 *J. Stat. Phys.* **64** 1017
[21] Trainoff S P and Cannell D S 2002 *Phys. Fluids* **14** 1340
[22] Bata L, Buka A and Janossy I 1974 *Solid State Commun.* **15** 647
[23] Blinov L M 1983 *Electro-Optical and Magneto-Optical Properties of Liquid Crystals* (New York: Wiley)
[24] Schneider U, de la Torre Juárez M, Zimmermann W and Rehberg I 1992 *Phys. Rev.* A **46** 1009
[25] Buka A, de la Torre Juárez M, Kramer L and Rehberg I 1989 *Phys. Rev.* A **40** 7427
Winkler B L, Richter H, Rehberg I, Zimmermann W, Kramer L and Buka A 1991 *Phys. Rev.* A **43** 1940
[26] Bodenschatz E, Zimmermann W and Kramer L 1988 *J. Physique* **49** 1875
[27] Press W H, Teukolsky S A, Vetterling W T and Flannery B P 1997 *Numerical Recipes in C* (Cambridge: Cambridge University Press) p 559f